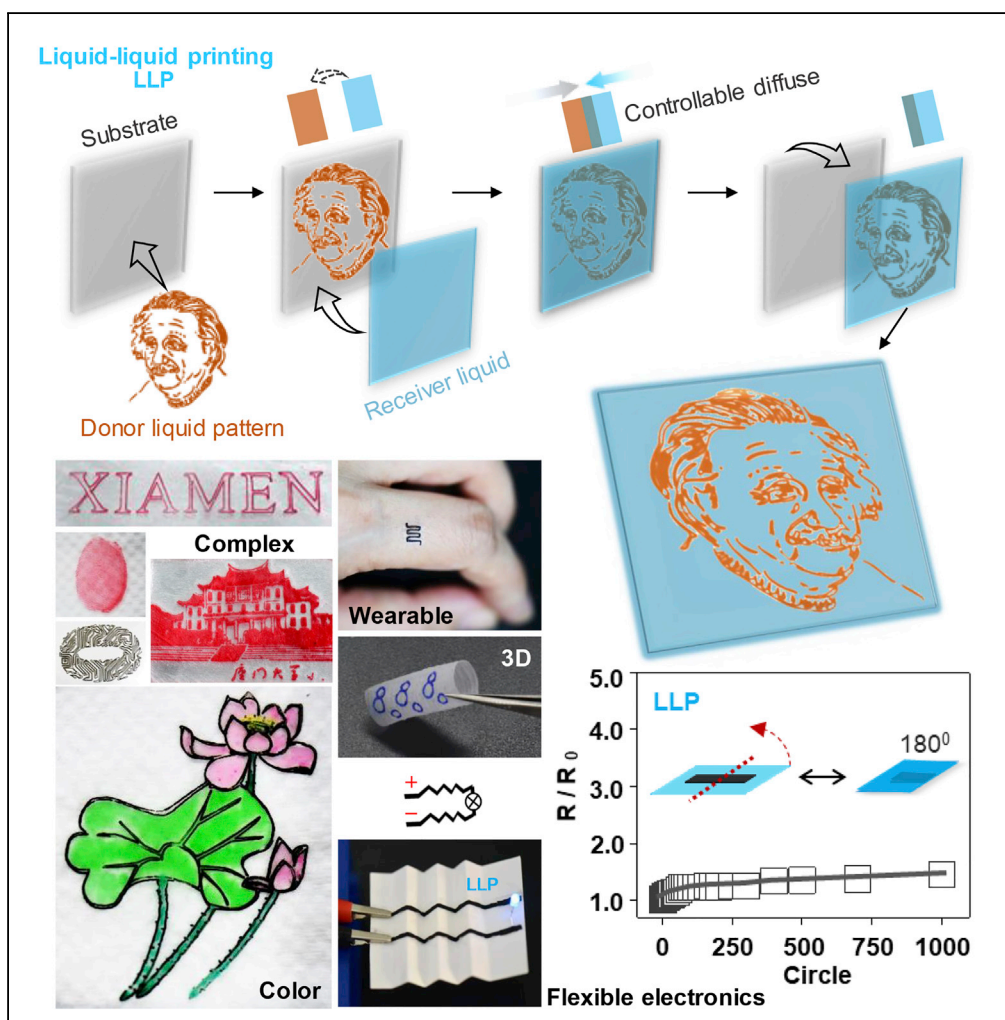


Article

Controllable Liquid-Liquid Printing with Defect-free, Corrosion-Resistance, Unrestricted Wetting Condition



Lingli Min, Haohui Zhang, Hong Pan, ..., Shuli Wang, Xinyu Chen, Xu Hou

houx@xmu.edu.cn

HIGHLIGHTS

A transfer printing mechanism based on miscible liquid-liquid interfaces

The material preparation and defect-free patterning can be synchronized

This printing mechanism is free of wetting constraint

Min et al., iScience 19, 93–100
 September 27, 2019 © 2019
 The Author(s).
<https://doi.org/10.1016/j.isci.2019.07.017>



Article

Controllable Liquid-Liquid Printing with Defect-free, Corrosion-Resistance, Unrestricted Wetting Condition

Lingli Min,^{1,2} Haohui Zhang,³ Hong Pan,¹ Feng Wu,² Yuhang Hu,³ Zhizhi Sheng,^{1,4} Miao Wang,² Mengchuang Zhang,² Shuli Wang,^{1,4} Xinyu Chen,¹ and Xu Hou^{1,2,4,5,6,*}

SUMMARY

Conventional printing is worth revisiting because of its established procedures in meeting the surging demand of manufacturing printed electronics, 3D products, etc. However, one goal in penetrating printing into these is to control pattern transfer with no limitation of wettability. Here we introduce a miscible liquid-liquid transfer printing mechanism that can synchronize material preparation and material patterning with desirable properties including limitless selection of raw materials, corrosion resistance, no wetting constraint, and ability to prepare large-area defect-free materials for multi-function applications. Theoretical modeling and experiments demonstrate that donor liquid could be used to make patterns within the bulk of a receiver material, allowing the obtained intrinsically patterned functional materials to be resistant to harsh conditions. Different from current liquid printing technologies, this printing approach enables stable and defect-free material preparation and is expected to prove useful in flexible display, soft electronics, 4D printing, and beyond.

INTRODUCTION

Printing has played a crucial role in promoting the development of human civilization (Fukuda and Someya, 2017; Kumar, 2015; Tian et al., 2013). Also, beyond publishing and transacting, nowadays “printing” is endowed with more roles in fulfilling myriad demands such as fabricating delicate structures and patterned functional materials (Feng et al., 2019; Fukuda and Someya, 2017; Kim et al., 2017; Parra-Cabrera et al., 2018; Raut and Al-Shamery, 2018; Schwartz and Boydston, 2019; Su et al., 2018). However, although printing holds great promises for fabricating and manufacturing patterned functional materials (Sun et al., 2015; Xia and Whitesides, 1998; Zhou and Song, 2011), the realization of functional properties of patterned materials such as tunability and mechanical and electrical stabilities heavily relies on not only the pattern delivering technologies but also the compatibility of the “donor patterns” and receiver materials (Carlson et al., 2012; Derby, 2010; Hoon et al., 2018; Hwang et al., 2010; Kumar, 2015; Lee et al., 2016; Liu et al., 2014; Meitl et al., 2006; Sun et al., 2015; Tian et al., 2013).

Driven by the demand of speed and precision in processes, and inspired from interface manipulation (Sun et al., 2015; Tumbleston et al., 2015; Villar et al., 2013), rapid progress has been made in liquid printing technologies based on immiscible interfaces, such as green plate-making technology (Bao et al., 2014; Zhou and Song, 2011), inkjet printing of concave microstructures (Bao et al., 2015), inkjet printing of embedded circuits (Jiang et al., 2016) and microchannels (Guo et al., 2015), all-liquid printing of microchannels (Feng et al., 2019), 3D microstructure fabrication via dynamic dewetting surfaces (Wang et al., 2015), and 3D printing of droplet networks or threads (Forth et al., 2018; Villar et al., 2013). However, even that the immiscible interfaces (Zeng et al., 2009) provide convenience in shaping delicate structures, it is limited in uniformity and integrity in fabricating intrinsically patterned materials, leading to compromises of functional properties. Moreover, another difficulty in optimizing the properties of patterned functional materials is that, an independent patterning process usually follows the material preparation (Lee et al., 2010). Therefore the integration of these two will benefit by saving time, ensuring structural integrity, and potentially enabling more application for intelligent manufacturing.

It is most commonly thought that liquid-liquid interfaces refer to the interfaces in immiscible systems (Hou et al., 2015; Zeng et al., 2009), due to their clear contact line and sustained phase boundaries. However, for printing applications based on immiscible systems, their material selections could be restricted, and

¹College of Chemistry and Chemical Engineering, Xiamen University, Xiamen 361005, China

²Research Institute for Biomimetics and Soft Matter, College of Physical Science and Technology, Xiamen University, Xiamen 361005, China

³George W. Woodruff School of Mechanical Engineering, Georgia Institute of Technology, Atlanta, GA 30332, USA

⁴Collaborative Innovation Center of Chemistry for Energy Materials, Xiamen University, Xiamen 361005, China

⁵State Key Laboratory of Physical Chemistry of Solid Surfaces, Xiamen University, Xiamen 361005, China

⁶Lead Contact

*Correspondence: houx@xmu.edu.cn

<https://doi.org/10.1016/j.isci.2019.07.017>



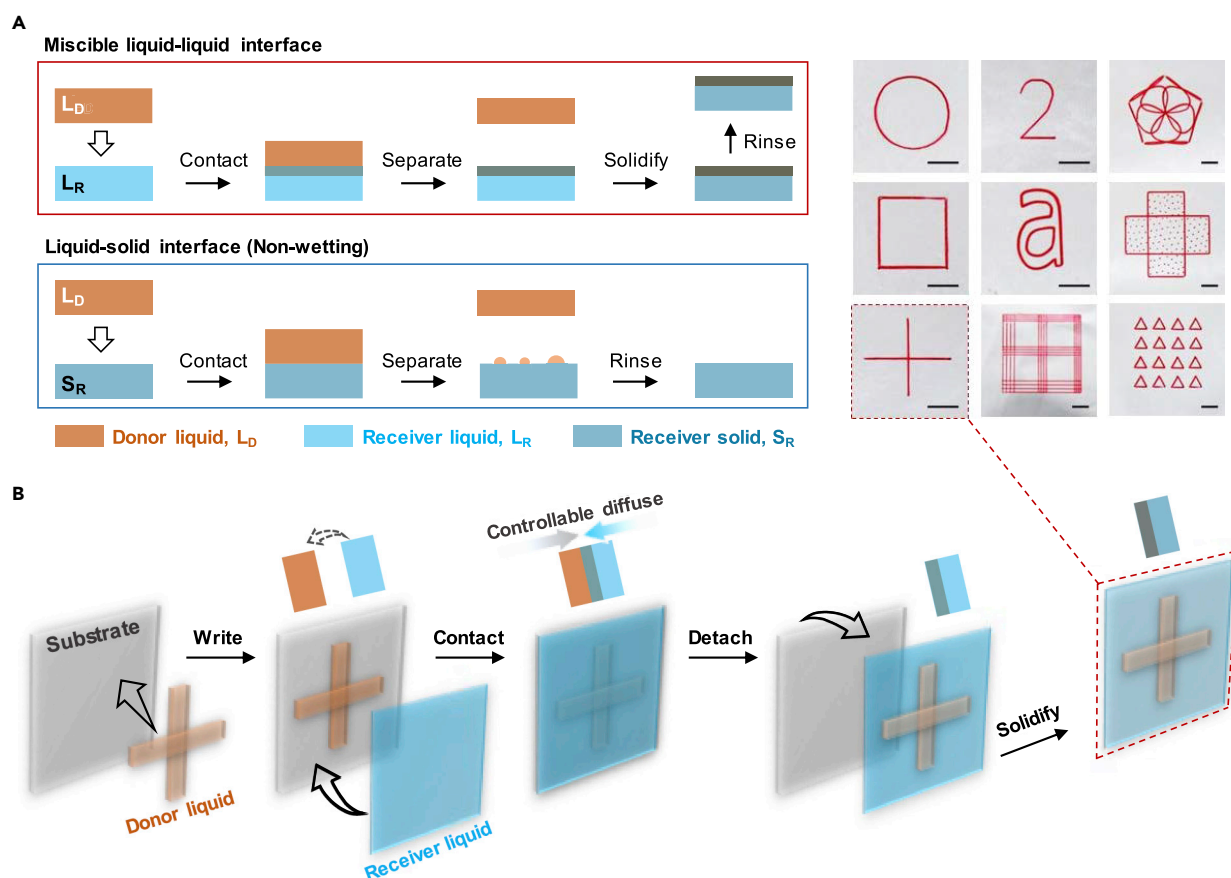


Figure 1. Liquid-Liquid Printing Mechanism for Synchronization of Material Preparation and Material Patterning

(A) Different behaviors of mass transfer at liquid-liquid and liquid-solid interfaces. S_R is the solid state of the receiver liquid (L_R), whereas S_D is the solid state of the donor liquid (L_D). For liquid-liquid interface, the donor liquid could spontaneously diffuse into the bulk of the receiver liquid. For liquid-solid interface, the donor could only stay on the surface of the receiver. See more details in Figure S1 and Table S1.

(B) Schematic illustration of a liquid-liquid printing process. See more details in Figure S2. Top right inset, intricately designed patterns with high resolution. The donor liquid is neutral red ink, and the receiver liquid is PVDF (acetone-DMAC) (Figure S3). Scale bars, 5 mm.

therefore most of them are derived from oil-aqueous solution systems (Forth et al., 2018; Villar et al., 2013). The miscible liquid-liquid interfaces have proved their usefulness in numerous industrial applications such as oil recovery and oil extraction (Vorobev, 2014). Distinct from those in immiscible systems, the dynamics involved with miscible liquid-liquid interfaces, even after agitating, are time variant and the interfaces in between would eventually disappear, leading to the whole homogeneity of mixture (Bai et al., 2018). This whole homogeneity is highly desirable in many manufacturing processes and can hardly be achieved in the immiscible systems. Also, the time-variant interfaces provide us with more possibilities in synchronizing multifunction. Here we show a liquid transfer printing approach, which employs the miscible liquid-liquid interfacial contact, through interfacial diffusion, and solidification, taking advantage of time variability of miscible interface, to achieve synchronization of designated material preparation with stable transfer printing without interfacial wettability restriction.

RESULTS AND DISCUSSION

Figure 1A contrasts the printing concept at different interfaces. For the liquid-liquid interface, the donor liquid starts to migrate into the receiver liquid after the contact between them, along with the solidification of the receiver, whereas for the liquid-solid interface (non-wetting system), the donor stays on the surface of the receiver. Owing to its high tunability in preparing dynamic liquid-liquid interface (Bai et al., 2018; Gonçalves et al., 2018; Jaworek, 2007; Rietveld et al., 2006), electrospray was selected to demonstrate our liquid-liquid printing concept. Figure 1B shows a typical process of our liquid-liquid printing for

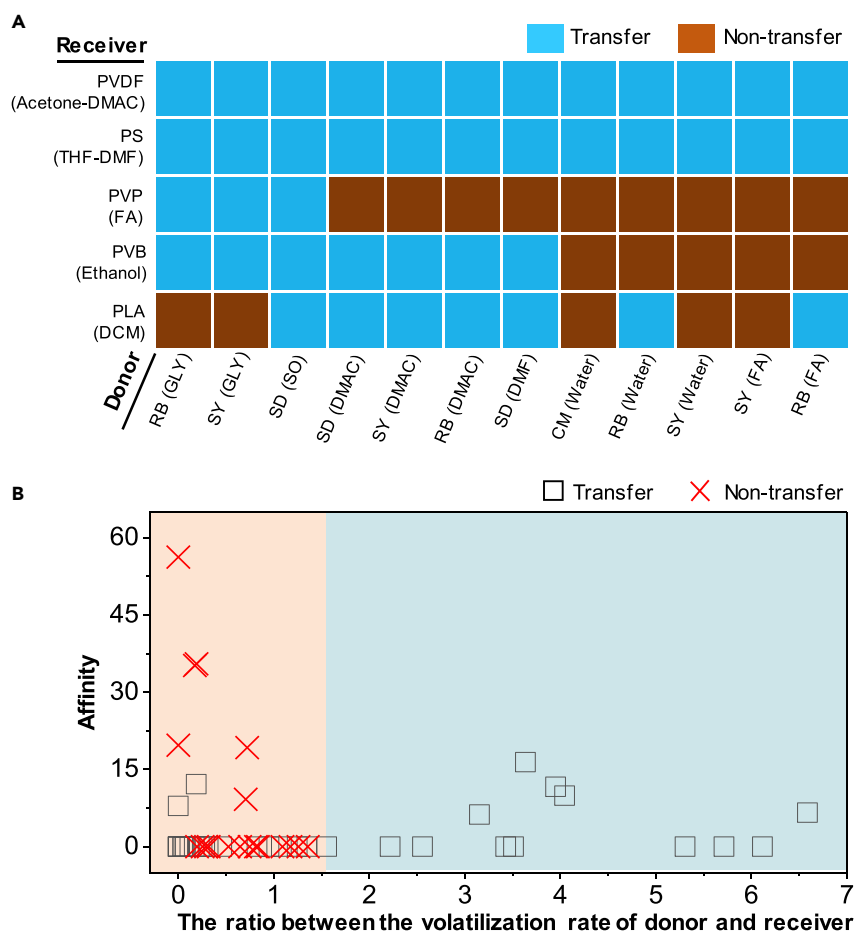


Figure 2. Data Matrix of 60 Pairs of Different Donor and Receiver Liquids

(A) The printing experimental results on 60 pairs of different donor and receiver liquids. The solvents are in the brackets following by the solutes. For example, donor RB (GLY) means GLY (GLYglycerin) is the donor solvent and RB is the donor solute. Other solvents include shell oil (SO), dimethylacetamide (DMAC), dimethylformamide (DMF), formic acid (FA), dichloromethane (DCM), and tetrahydrofuran (THF). The corresponding solutes include polystyrene (PS), polylactic acid (PLA), polyvinyl butyral (PVB), polyvinylpyrrolidone (PVP), sunset yellow (SY), carmine (CM) and Sudan red (SD).

(B) The ratio between the volatilization rate of the donor and receiver with regard to the affinity between the donor and receiver. Volatilization rate is the mass reduction of the liquids divided by the elapsed time whereby the liquid is vaporized (Table S2). The affinity is obtained by dividing the value of receding angle by the solubility level of the donor solute in the receiver solvent (Tables S3 and S4). The experiments show that in the cyan shading area, the pattern transfers at the liquid-liquid interface have higher possibilities to be achieved, whereas in the pink shading area some of them may not be achieved.

synchronization of material preparation. Compared with the conventional printing, our liquid-liquid printing excels in non-wetting systems (Video S1). When we chose a red dye aqueous rhodamine B solution (RB) as donor, and PVDF (acetone-DMAC) (polyvinylidene fluoride with acetone-dimethylacetamide) as receiver, RB could not sustain on the surface of solid PVDF, due to the hydrophobic surface of the solid PVDF. However, liquid-liquid printing has no such limitation, because the liquid interface could let the aqueous dye into the liquid PVDF (acetone-DMAC) before its solidification. Thus our liquid-liquid printing approach with the unrestricted wetting condition would expand the scope of printing materials.

Figure 2A shows our data matrix from printing experiments of 60 pairs of different donor and receiver liquids, among which 41 work well. We found that when the receiver liquids are highly volatile, it is difficult for pattern transfer between the interfaces because of the quicker evaporation of the solvents, which leaves behind the solid-solid or the solid-liquid contact rather than the liquid-liquid contact. The affinity between the two liquids depends on their mutual solubility. For example, carmine with deionized (DI) water could

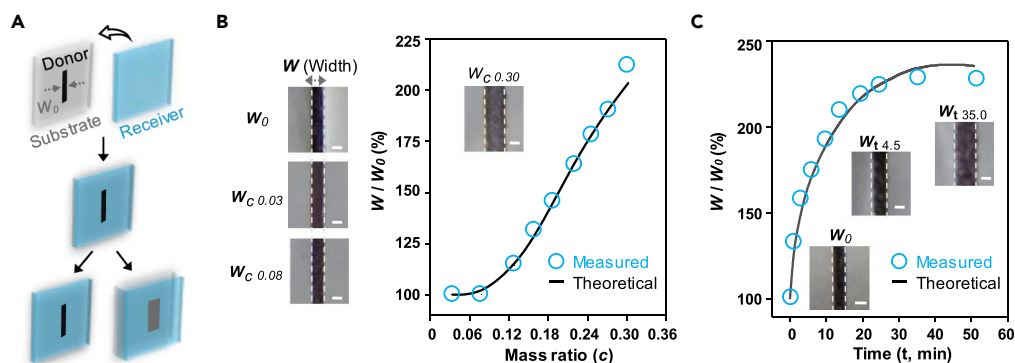


Figure 3. Pattern Size Tuning of Liquid-Liquid Printing

(A) Schematic diagram of the diffusion model. W_0 is the original width of the pattern line.

(B) Mass ratio of the receiver solvent to the overall receiver, i.e., c , regulates the printing line width. It is determined by mass flow rate (Table S6). The liquid receiver is PVDF (acetone-DMAC) (Figure S4A), whereas the liquid donor is black neutral pen ink (Figure S4B). W_c is the width of the line for a special c . The blue circles are experimental data for the ratio between W_c and W_0 , whereas the black curve represents the model results. Scale bars, 0.5 mm. The experiments are conducted at 25°C and 35% \pm 3% relative humidity.

(C) The diffusion time regulates the printing line width. W_t is the width of the line at a certain time (t). The blue circles are experimental data for the ratio between W_t and W_0 , whereas the black curve represents the theoretical simulation results. Scale bars, 0.5 mm.

not be used as the donor material to make patterns inside the receiver liquid of polylactic acid (PLA) with dichloromethane (DCM), as they are immiscible liquids. However, when the soluble receiver liquid, such as polystyrene with tetrahydrofuran-dimethylformamide was selected, it worked. Deriving from the above, it is thought that the two factors accountable to realize the synchronization of material preparation and material patterning by liquid-liquid printing are volatility and affinity.

The ratio between the volatilization rates of the donor and receiver liquids was further investigated with regard to a certain affinity between the two liquids (Figure 2B). It is noted that the slower the receiver liquid volatilizes, the easier the donor can deliver into it. When the ratio is above 1.55, meaning the volatilization rate of the donor liquid is at least 1.55 times the volatilization rate of receiver, pattern transfer at the liquid-liquid interface could be well achieved. For instance, when RB is used as a donor liquid, if we choose polyvinylpyrrolidone with formic acid as the receiver liquid, the ratio of volatilization of which is 0.72, the donor liquid material cannot deliver into the receiver; if we choose the liquid PVDF (acetone-DMAC) as the receiver liquid, the ratio of which is 4.00, the pattern of donor liquid can be printed into the receiver. Incomplete transfer can occur in the immiscible systems due to the solvent extraction effect. For example, the donor liquid RB can also be partly transferred into the receiver liquid PLA with DCM, because of the higher solubility of RB in dichloromethane than DI water.

The diffusivity property on the miscible liquid-liquid interfaces between two materials plays a big part in controlling the size of patterns obtained through our liquid-liquid printing mechanism, as after the contact, the donor liquid patterns tend to expand. Two parameters are employed to realize accurate sizes of the patterns. One is the mass ratio of the receiver solvent to the overall receiver (c) and the other is the contact time between the donor and the receiver. Here we selected a line pattern to demonstrate how to obtain the original or the extended width (Figure 3A). Figure 3B illustrates the ratio of the width change before and after printing by increasing c . When c is below 0.08, the ratio is at 1 to achieve the original pattern size printing, whereas when c is above 0.08, the ratio increases rapidly with the increase of c .

A theoretical model is established on the underlying mechanism of quality and controllable mass transfer under our liquid-liquid printing system. The donor liquid (L_D) that is composed of solvent (L_{DS}) and solute (ink pigment) is mixed with the receiver liquid (L_R) that is composed of solvent (L_{RS}) and solute (polymers, L_{RP}) in the vicinity of contact. First, we studied the diffusion of the donor solvent in the receiver. When the mass ratio of the receiver solvent to the overall receiver (c) is low, the diffusion of the donor solvent is

primarily dominated by diffusing through the polymers in the receiver, whereas when c is high, the donor solvent can diffuse into the receiver easier with the facility of the solvent in the receiver. Therefore, the diffusivity of the donor solvent in the receiver is defined as follows:

$$a(c) = \begin{cases} D_{1\text{poly}} & c < c_{\text{cri}} \\ \frac{(D_{1\text{solv}} - D_{1\text{poly}})}{2} \left[1 - \cos\left(\frac{\pi}{1 - c_{\text{cri}}}(c - c_{\text{cri}})\right) \right] + D_{1\text{poly}} & c_{\text{cri}} < c < 1 \end{cases} \quad (\text{Equation 1})$$

where $D_{1\text{solv}}$ is the diffusion coefficient of the pure donor solvent in the receiver solvent L_{RS} , $D_{1\text{poly}}$ is the diffusion coefficient of the pure donor solvent in the receiver polymer L_{RP} , and c_{cri} is the critical mass ratio of the receiver solvent to the overall receiver for the receiver solvent to start promoting the diffusion of the donor solvent (Table S5). Next, we studied the diffusion of the donor ink solute in the receiver, for which we referred to a theoretical model proposed by Kunii (Kunii et al., 1995), and define the diffusivity of the ink solute as

$$Z(g/f, c) = \begin{cases} D_0(c) & g/f < Z_0 \\ \frac{ra(c)}{2} \left[1 - \cos\left(\frac{\pi}{(Z_1 - Z_0)}\left(\frac{g}{f} - Z_0\right)\right) \right] + D_0(c) & Z_0 < g/f < Z_1 \\ ra(c) & g/f > Z_1 \end{cases} \quad (\text{Equation 2})$$

where g is the density of the donor solvent and f is the density of the donor ink solute and Z_0 and Z_1 are two constants determining the drag of solvent on solute. When g/f is smaller than Z_0 , the flow of the donor liquid is not sufficient enough to accelerate the flow of the ink solute in the donor into the receiver. In this case, the diffusion coefficient of the ink solute is $D_0(c)$, which has a similar form as Equation 1. If g/f is bigger than Z_1 , the donor ink solute will move with the donor liquid. However, due to the resistance of the polymers, the diffusion coefficient of the ink solute in the donor is smaller than that of the donor liquid by a factor r that is smaller than 1. If g/f is in between, we use a cosine function as the transition curve for the diffusion coefficient of the ink solute. As shown in Figure 3B, as the solvent content in the receiver c increases, it promotes more ink solute to diffuse into the donor, and thus the width of the print is wider. This model also captures the kinetic process. As shown in Figure 3C, the width of the print is plotted as a function of time. As time increases, the width of the print increases and eventually reaches a plateau value. The experimental results and theoretical predictions agree well, and this model can be used for the quantitative system design.

Our liquid-liquid printing can be used to prepare universally durable patterned materials (Figure 4A and S5, and Video S1), and these prepared materials are very stable, even under harsh conditions (Figure 4B). We further demonstrate its application scopes by realizing complex printing (Figures 4C, S6, and S7A), colorful printing (Figures 4C and S7B), multifunctional printing (Figures S7C–S7E), and 3D printing (Figures 4C and S8). Our approach also shows promise in making flexible circuits (Video S2). Compared with the conventional circuits' liquid-solid printing (LSP), the circuits' liquid-liquid printing (LLP) shows lower resistivity (Figures 4D and S9), better mechanical flexibility (Figure 4E), and durability (Figure 4F) during the folding process. Because of the dewetting property of the aqueous ink donor on the hydrophobic receiver solid, LSP left behind many cracks on the surface of the final products, whereas LLP left behind a smooth surface without cracks (see Figures 4G, S10, and S11). Moreover, our approach can be used to prepare waterproof circuits (Figure S12, Video S2). Therefore, this printing approach opens possibilities in building stable, defect-free, non-wetting, waterproof printing technology for huge demand in deformable circuits.

Conclusion

In summary, we show a new liquid-liquid printing capable of achieving the synchronization of material preparation and durable material pattern without wetting constraint. This mechanism realizes a controllable pattern transfer by miscible liquid-liquid interfacial contact, diffusion, and solidification. By our experimental results and theoretical modeling, there are 60 combination experiments with 41 combinations of liquid-liquid printing that work well. The main reasons for the remaining unworkable combinations are two key factors: volatility and affinity. We found the critical value of liquid-liquid printing as the ratio of

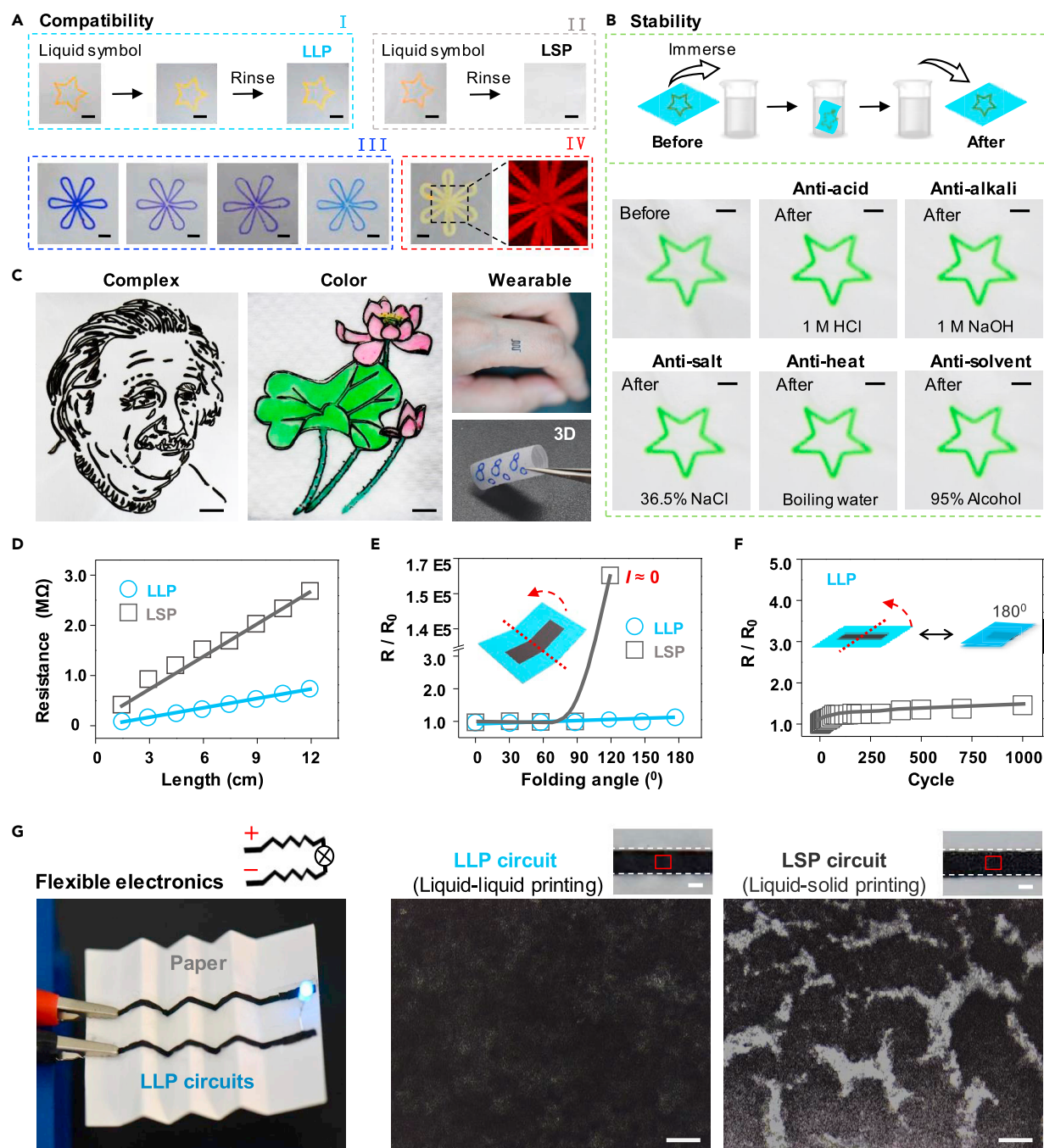


Figure 4. Advantages and Applications of Liquid-Liquid Printing

(A) Compatibility. The liquid-liquid printing (LLP) symbol could withstand surface rinsing (I), whereas the same liquid-solid printing (LSP) symbol disappeared after surface rinsing (II). LLP is compatible with various donor liquids (III). From left, oily gel donor, ballpoint pen ink donor, and two aqueous gel donors. A fluorescent donor (IV). The right inset is a magnified fluorescence photograph. Scale bars, 5 mm.

(B) Stability. Schematic illustration (top) of the treatment process and optical images (middle and bottom) of the LLP stars before and after immersing into the strong acid, strong alkali, salt brine, boiling water, and the organic solvent. Scale bars, 3 mm.

(C) Examples of intricately designed patterns by liquid-liquid printing: complex, colorful, wearable, and three-dimensional (3D) products. Scale bars, 5 mm.

(D) The length-resistance tests of the conductive circuits prepared by LLP and LSP.

(E) Relative resistance of printing circuits folded under various folding angles. The inset is the schematic illustration of the bending tests. The LLP circuits (thickness 54 μm) achieve better mechanical flexibility, whereas the LSP circuits (thickness 64 μm) broke when bending to 120 $^\circ$.

Figure 4. Continued

(F) The relative resistance change of the LLP flexible circuits as a function of the folding times under 180° folding angle.

(G) A light-emitting diode device connected by LLP flexible and transparent circuits, which were supported on a paper (left). Zoomed-in view of the surface morphology of the LLP and LSP circuits (right). LLP circuits show a smooth surface after drying, whereas LSP circuits have many cracks on the surface. Scale bars, 1 mm (top) and 100 μm (bottom).

liquid volatilization rate is 1.55. Controllable printing is expected to be achieved by liquid-liquid interface behavior. It was assumed that two effective ways in our system to get controllable sizes of patterns are by utilizing the mass ratio of the receiver solvent and the diffusion time. Our approach is applicable to miscible liquid-liquid system and breaks the limitation of printing materials in the non-wetting system. Moreover, it has great potentials in defect-free material preparations for many applications such as durable and deformable electrical circuits, flexible and wearable devices, electronic displays, and many other applications beyond publishing, packaging, and manufacturing.

Limitations of Study

When the volatilization rate of the donor liquid is at least 1.55 times that of the receiver, pattern transfer at the liquid-liquid interface can be ensured. This is obtained through 60 pairs of donor and receiver liquids in our study, so we do not know if the ratio can vary with more different samples.

METHODS

All methods can be found in the accompanying [Transparent Methods supplemental file](#).

SUPPLEMENTAL INFORMATION

Supplemental Information can be found online at <https://doi.org/10.1016/j.isci.2019.07.017>.

ACKNOWLEDGMENTS

This work was supported by the National Key R&D Program of China (2018YFA0209500), the National Natural Science Foundation of China (21673197, 21621091, 51706191, 21808191), Young Overseas High-level Talents Introduction Plan, the 111 Project (B16029), the Fundamental Research Funds for the Central Universities in China (20720190037, 20720170050), the Natural Science Foundation of Fujian Province of China (No. 2018J06003), and Special Project of Strategic Emerging Industries from Fujian Development and Reform Commission. The authors thank W. Chen, Y. Chi, Y. Fan, and S. Chen for discussion and help.

AUTHOR CONTRIBUTIONS

X.H. conceived the idea. X.H. and L.M. designed the research. L.M., H.P., and F.W. performed the experiments. Y.H. and H.Z. built the mathematical model. X.H., L.M., H.P., Y.H., H.Z., F.W., Z.S., M.W., M.Z., S.W., and X.C. analyzed and interpreted the results. X.H., L.M., H.Z., and X.C. drafted the manuscript, and all authors contributed to the writing of the manuscript.

DECLARATION OF INTERESTS

The authors declare no competing interests.

Received: May 5, 2019

Revised: July 9, 2019

Accepted: July 12, 2019

Published: September 27, 2019

REFERENCES

Bai, X.-J., Chen, D., Li, L.-L., Shao, L., He, W.-X., Chen, H., Li, Y.-N., Zhang, X.-M., Zhang, L.-Y., Wang, T.-Q., et al. (2018). Fabrication of MOF thin films at miscible liquid-liquid interface by spray method. *ACS Appl. Mater. Interfaces* *10*, 25960–25966.

Bao, B., Jiang, J., Li, F., Zhang, P., Chen, S., Yang, Q., Wang, S., Su, B., Jiang, L., and Song, Y. (2015).

Fabrication of patterned concave microstructures by inkjet imprinting. *Adv. Funct. Mater.* *25*, 3286–3294.

Bao, B., Su, B., Wang, S., Chen, S., Wu, L., Jia, Z., Song, Y., and Jiang, L. (2014). Stretching velocity-dependent dynamic adhesion of the water/oil interfaces for high quality lithographic printing. *Adv. Mater. Interfaces* *1*, 1400080.

Carlson, A., Bowen, A.M., Huang, Y., Nuzzo, R.G., and Rogers, J.A. (2012). Transfer printing techniques for materials assembly and micro/nanodevice fabrication. *Adv. Mater.* *24*, 5284–5318.

Derby, B. (2010). Inkjet printing of functional and structural materials: fluid property requirements, feature stability, and resolution. *Annu. Rev. Mater. Res.* *40*, 395–414.

- Feng, W., Chai, Y., Forth, J., Ashby, P.D., Russell, T.P., and Helms, B.A. (2019). Harnessing liquid-in-liquid printing and micropatterned substrates to fabricate 3-dimensional all-liquid fluidic devices. *Nat. Commun.* *10*, 1095.
- Forth, J., Liu, X., Hasnain, J., Toor, A., Miszta, K., Shi, S., Geissler, P.L., Emrick, T., Helms, B.A., and Russell, T.P. (2018). Reconfigurable printed liquids. *Adv. Mater.* *30*, 1707603.
- Fukuda, K., and Someya, T. (2017). Recent progress in the development of printed thin-film transistors and circuits with high-resolution printing technology. *Adv. Mater.* *29*, 1602736.
- Goncalves, R., Cardoso, V.F., Pereira, N., Oliveira, J., Nunes-Pereira, J., Costa, C.M., and Lanceros-Mendez, S. (2018). Evaluation of the physicochemical properties and active response of piezoelectric poly(vinylidene fluoride-co-trifluoroethylene) as a function of its microstructure. *J. Phys. Chem. C* *122*, 11433–11441.
- Guo, Y., Li, L., Li, F., Zhou, H., and Song, Y. (2015). Inkjet print microchannels based on a liquid template. *Lab Chip* *15*, 1759–1764.
- Hoon, Y., Minho, S., Kahyun, S., Insol, H., Kangseok, L., Chaenyung, C., Tae-il, K., and Eui, J.H. (2018). Wet-responsive, reconfigurable, and biocompatible hydrogel adhesive films for transfer printing of nanomembranes. *Adv. Funct. Mater.* *28*, <https://doi.org/10.1002/adfm.201706498>.
- Hou, X., Hu, Y., Grinthal, A., Khan, M., and Aizenberg, J. (2015). Liquid-based gating mechanism with tunable multiphase selectivity and antifouling behaviour. *Nature* *519*, 70–73.
- Hwang, J.K., Cho, S., Dang, J.M., Kwak, E.B., Song, K., Moon, J., and Sung, M.M. (2010). Direct nanoprining by liquid-bridge-mediated nanotransfer moulding. *Nat. Nanotechnol.* *5*, 742–748.
- Jaworek, A. (2007). Electro spray droplet sources for thin film deposition. *J. Mater. Sci.* *42*, 266–297.
- Jiang, J., Bao, B., Li, M., Sun, J., Zhang, C., Li, Y., Li, F., Yao, X., and Song, Y. (2016). Fabrication of transparent multilayer circuits by inkjet printing. *Adv. Mater.* *28*, 1420–1426.
- Kim, J., Kumar, R., Bhandodkar, A.J., and Wang, J. (2017). Advanced materials for printed wearable electrochemical devices: a review. *Adv. Electron. Mater.* *3*, 1600260.
- Kumar, S. (2015). Liquid transfer in printing processes: liquid bridges with moving contact lines. *Annu. Rev. Fluid Mech.* *47*, 67–94.
- Kunii, T.L., Nosovskij, G.V., and Hayashi, T. (1995). A diffusion model for computer animation of diffuse ink painting. In *Proceedings of the Computer Animation (IEEE Computer Society)*, pp. 98.
- Lee, C.H., Kim, D.R., and Zheng, X.L. (2010). Fabricating nanowire devices on diverse substrates by simple transfer-printing methods. *Proc. Natl. Acad. Sci. U S A* *107*, 9950–9955.
- Lee, H., Um, D.-S., Lee, Y., Lim, S., Kim, H.-j., and Ko, H. (2016). Octopus-inspired smart adhesive pads for transfer printing of semiconducting nanomembranes. *Adv. Mater.* *28*, 7457–7465.
- Liu, M., Wang, J., He, M., Wang, L., Li, F., Jiang, L., and Song, Y. (2014). Inkjet printing controllable footprint lines by regulating the dynamic wettability of coalescing ink droplets. *ACS Appl. Mater. Interfaces* *6*, 13344–13348.
- Meitl, M.A., Zhu, Z.T., Kumar, V., Lee, K.J., Feng, X., Huang, Y.Y., Adesida, I., Nuzzo, R.G., and Rogers, J.A. (2006). Transfer printing by kinetic control of adhesion to an elastomeric stamp. *Nat. Mater.* *5*, 33–38.
- Parra-Cabrera, C., Achille, C., Kuhn, S., and Ameloot, R. (2018). 3D printing in chemical engineering and catalytic technology: structured catalysts, mixers and reactors. *Chem. Soc. Rev.* *47*, 209–230.
- Raut, N.C., and Al-Shamery, K. (2018). Inkjet printing metals on flexible materials for plastic and paper electronics. *J. Mater. Chem. C* *6*, 1618–1641.
- Rietveld, I.B., Kobayashi, K., Yamada, H., and Matsushige, K. (2006). Electro spray deposition, model, and experiment: toward general control of film morphology. *J. Phys. Chem. B* *110*, 23351–23364.
- Schwartz, J.J., and Boydston, A.J. (2019). Multimaterial actinic spatial control 3D and 4D printing. *Nat. Commun.* *10*, 791.
- Su, M., Huang, Z.D., Li, Y.F., Qian, X., Li, Z., Hu, X.T., Pan, Q., Li, F.Y., Li, L.H., and Song, Y.L. (2018). A 3D self-shaping strategy for nanoresolution multicomponent architectures. *Adv. Mater.* *30*, 8.
- Sun, J., Bao, B., He, M., Zhou, H., and Song, Y. (2015). Recent advances in controlling the depositing morphologies of inkjet droplets. *ACS Appl. Mater. Interfaces* *7*, 28086–28099.
- Tian, D.L., Song, Y.L., and Jiang, L. (2013). Patterning of controllable surface wettability for printing techniques. *Chem. Soc. Rev.* *42*, 5184–5209.
- Tumbleston, J.R., Shirvanyants, D., Ermoshkin, N., Januszewicz, R., Johnson, A.R., Kelly, D., Chen, K., Pinschmidt, R., Rolland, J.P., Ermoshkin, A., et al. (2015). Continuous liquid interface production of 3D objects. *Science* *347*, 1349–1352.
- Villar, G., Graham, A.D., and Bayley, H. (2013). A tissue-like printed material. *Science* *340*, 48–52.
- Vorobev, A. (2014). Dissolution dynamics of miscible liquid/liquid interfaces. *Curr. Opin. Colloid Interface Sci.* *19*, 300–308.
- Wang, L., Li, F., Kuang, M., Gao, M., Wang, J., Huang, Y., Jiang, L., and Song, Y. (2015). Interface manipulation for printing three-dimensional microstructures under magnetic guiding. *Small* *11*, 1900–1904.
- Xia, Y.N., and Whitesides, G.M. (1998). Soft lithography. *Annu. Rev. Mater. Sci.* *28*, 153–184.
- Zeng, H., Tian, Y., Zhao, B., Tirrell, M., and Israelachvili, J. (2009). Friction at the liquid/liquid interface of two immiscible polymer films. *Langmuir* *25*, 4954–4964.
- Zhou, H.H., and Song, Y.L. (2011). Green plate making technology based on nano-materials. *Adv. Mater. Res.* *174*, 447–449.

ISCI, Volume 19

Supplemental Information

**Controllable Liquid-Liquid Printing
with Defect-free, Corrosion-
Resistance, Unrestricted Wetting Condition**

Lingli Min, Haohui Zhang, Hong Pan, Feng Wu, Yuhang Hu, Zhizhi Sheng, Miao Wang, Mengchuang Zhang, Shuli Wang, Xinyu Chen, and Xu Hou

Supplemental data

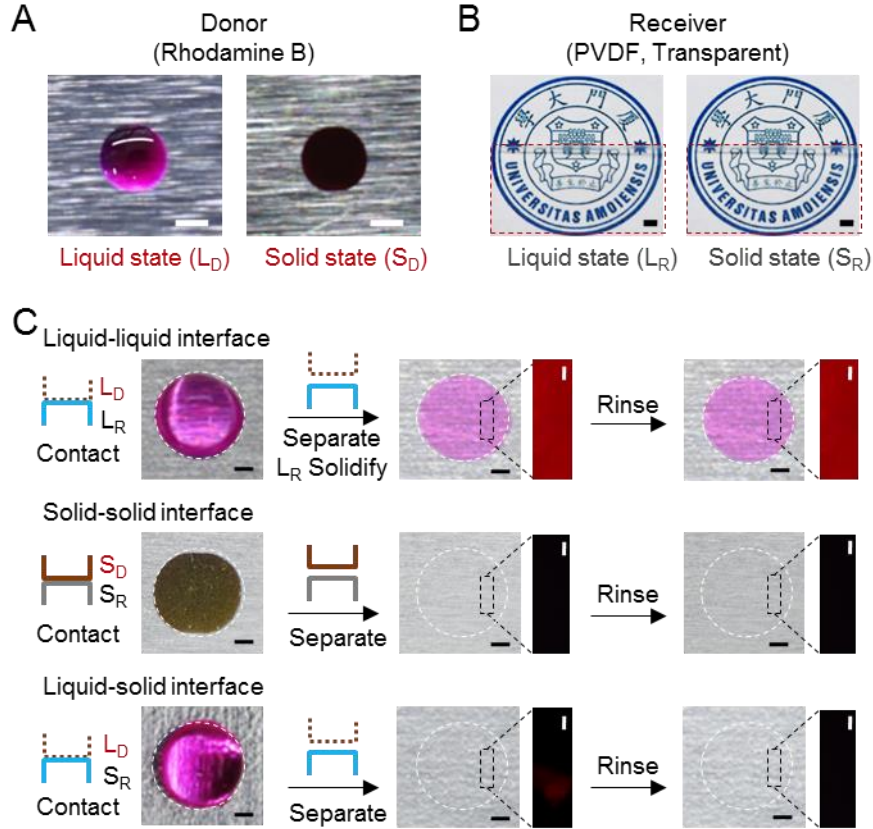


Figure S1. Substance transfer behaviors at different interfaces. (A) Photos of a donor liquid, Rhodamine B (RB) aqueous solution. L_D/S_D indicates the liquid/solid state of the donor. Scale bars: 0.5 mm. (B) Photos of a transparent PVDF receiver. L_R/S_R indicates the liquid/solid state of the receiver. The liquid state of the receiver is PVDF (acetone-DMAC). Scale bars: 0.5 mm. (C) Comparison of the stabilities among different printing approaches for substance transfer at liquid-liquid, solid-solid, and solid-liquid interfaces. The right insets (fluorescence images) show that only liquid-liquid interface delivered RB into PVDF receiver in the non-wetting system. Scale bars: 0.2 mm. Right insets scale bars: 50 μm . Related to Figure 1.

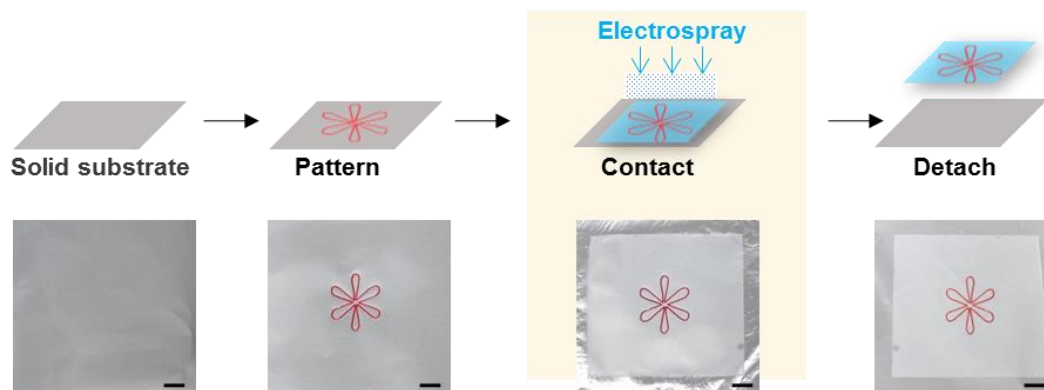


Figure S2. A typical liquid-liquid printing process *via* the electro spray. A pattern with donor liquid was written on a substrate (aluminum foil). During the electro spray process, the cross was transferred and delivered into the liquid receiver. The printed product could be easily peeled off from the donor substrate before or after the full solidification of the receiver. Scale bars: 5 mm. Related to Figure 1.

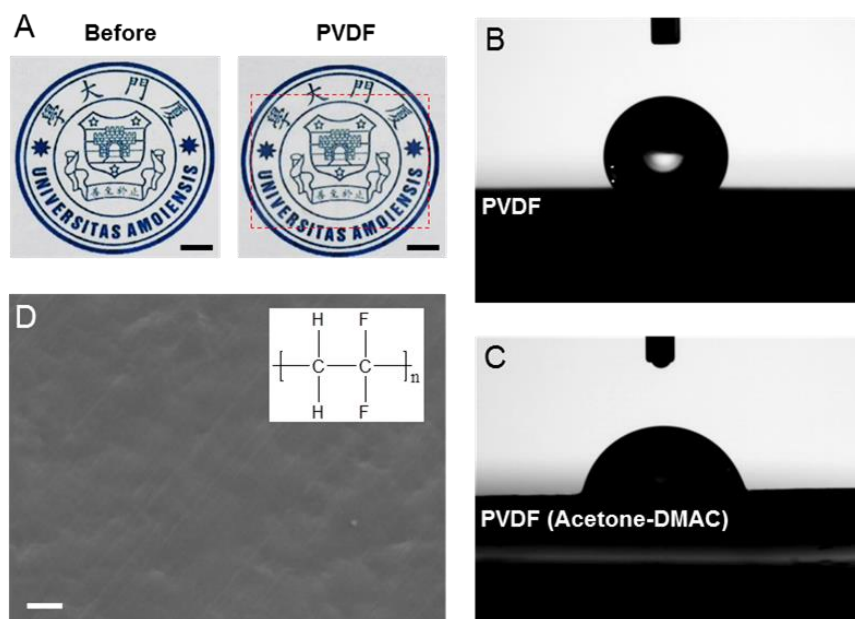


Figure S3. Characterization of the PVDF receiver. (A) Optical photos indicate the high transparency of the PVDF receiver (solid state, thickness, 3 μm). Scale bars, 5 mm. (B) The water contact angle of the solid state of PVDF. (C) The water receding angle of the liquid state of PVDF (acetone-DMAC). (D) The SEM image of the solid state of PVDF. Scale bar: 50 μm . Related to Figure 1.

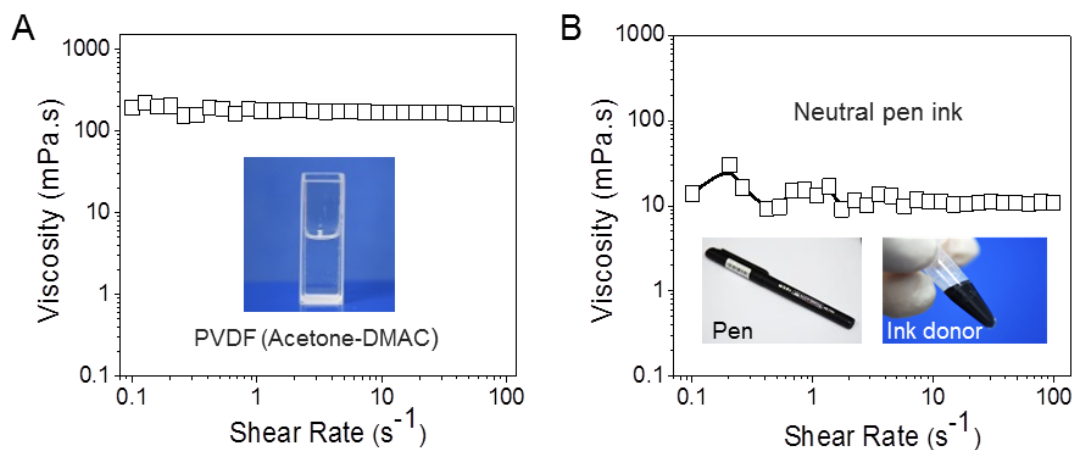


Figure S4. Rheological behavior of the receiver PVDF (acetone-DMAC) (A) and the neutral pen ink (B) used for Figure 3. Related to Figure 3.

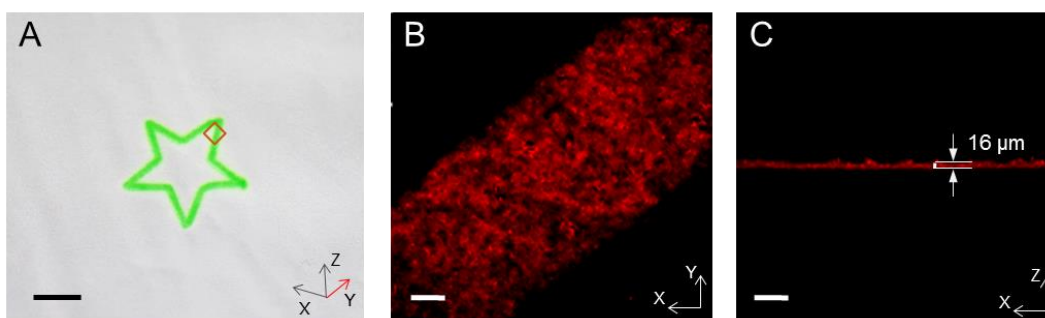


Figure S5. Characterization of the printed materials with star pattern in Figure 4B. (A) The liquid-liquid printing star after surface rinsing. (B, C) Laser confocal microscopy shows the 3D distribution of the donor solute in the receiver. The thickness of the receiver is 16 μm . Scale bars: 5 mm (A) and 100 μm (B and C). Related to Figure 4.

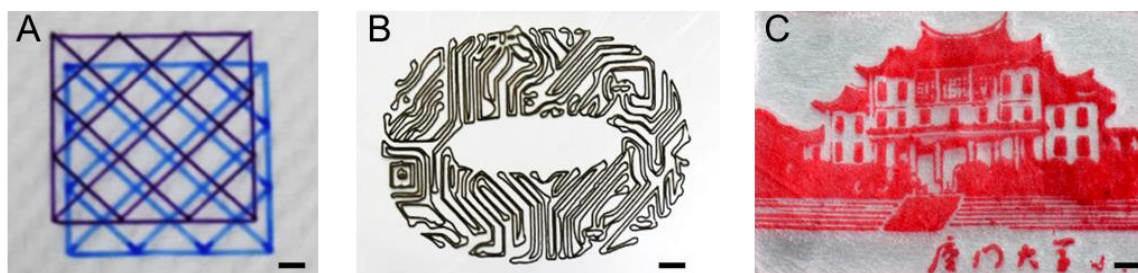


Figure S6. Examples of the liquid-liquid printing complex patterns. Crosslines (A), circular circuit pattern (B), the south auditorium building of Xiamen University (C). Scale bars: 5 mm. Related to Figure 4.

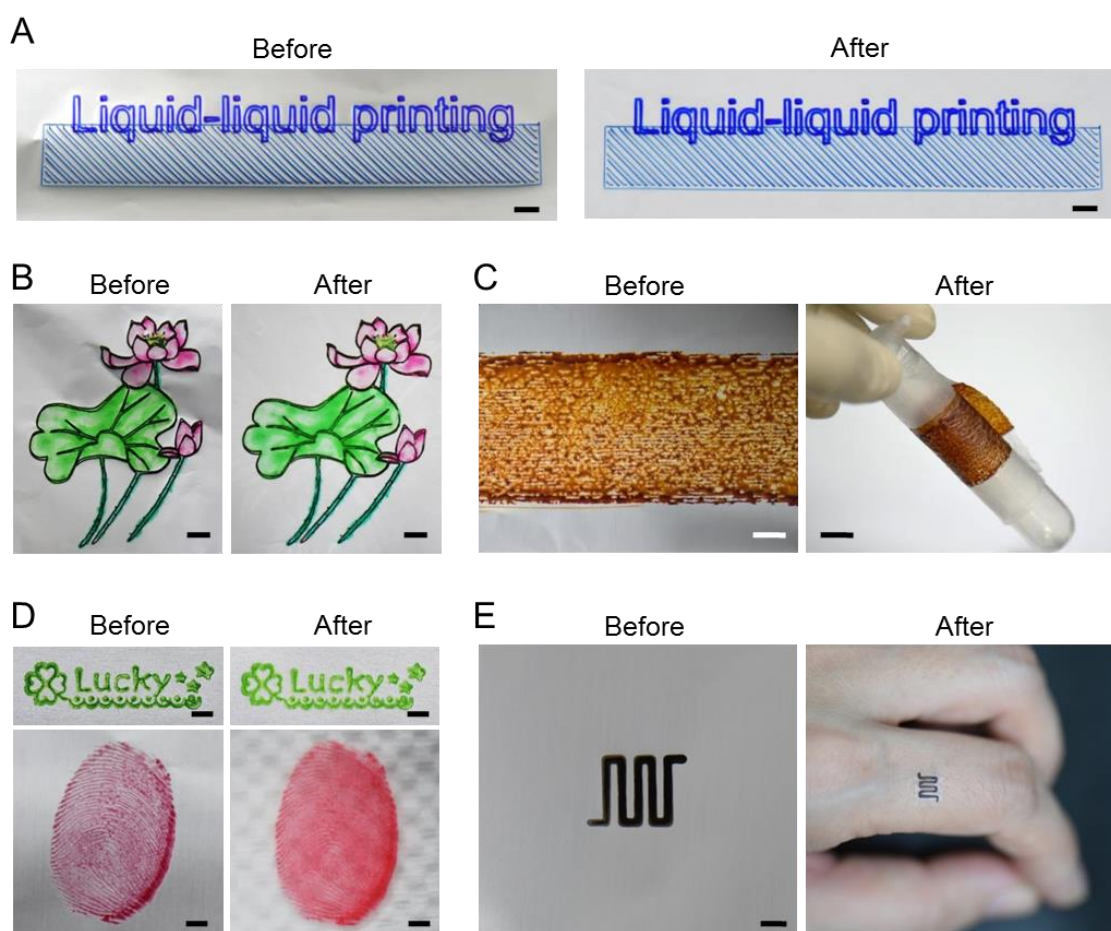


Figure S7. Various donor patterns before and after the liquid-liquid printing. A neutral gel pen donor (A), a color ink donor (B), an aqueous ferrofluid donor (C), a seal oil donor (D), and a lab-made composite donor (E). The printed products with the aqueous ferrofluid (C) and the lab-made composite donor (E) were attached to a centrifuge tube and a finger, respectively. Scale bars: 5 mm (A-C), 2 mm (D and E). Related to Figure 4.

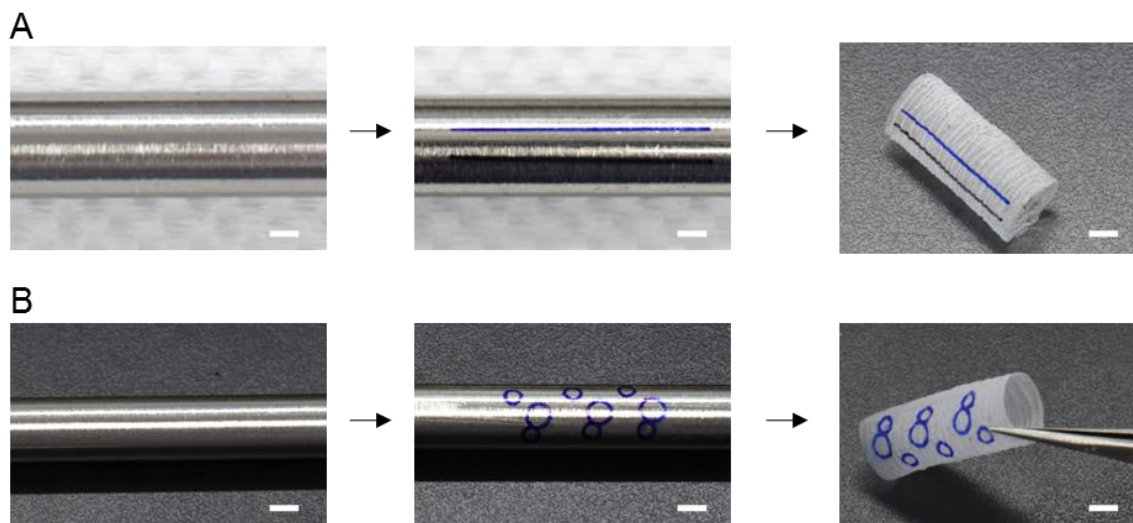


Figure S8. Typical processes of the liquid-liquid printing 3D structures. The Liquid-liquid printing achieves synchronization of 3D material preparation and inner patterning of lines (A) and circles (B). Scale bars: 3 mm. Related to Figure 4.

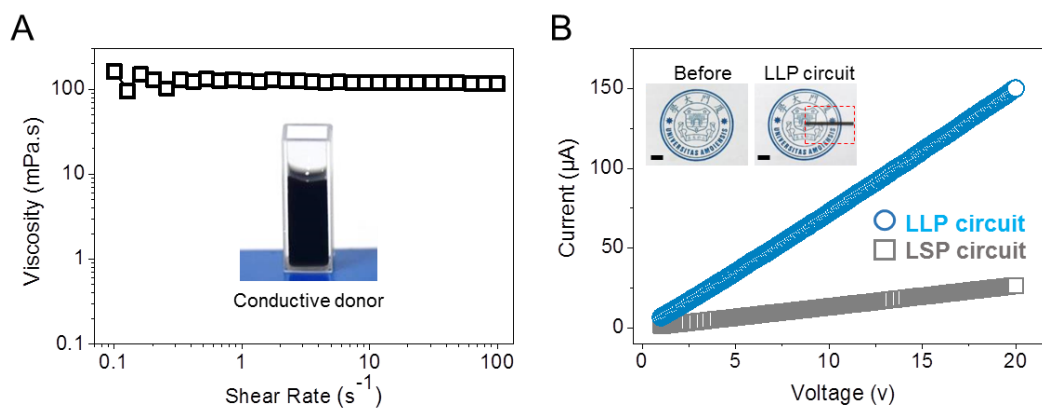


Figure S9. (A) Rheological behavior of the conductive donor. (B) The voltage-current tests of the printed circuits. Insets show the macroscopic optical images of the liquid-liquid printing flexible circuits. Scale bars, 5 mm. Related to Figure 4.

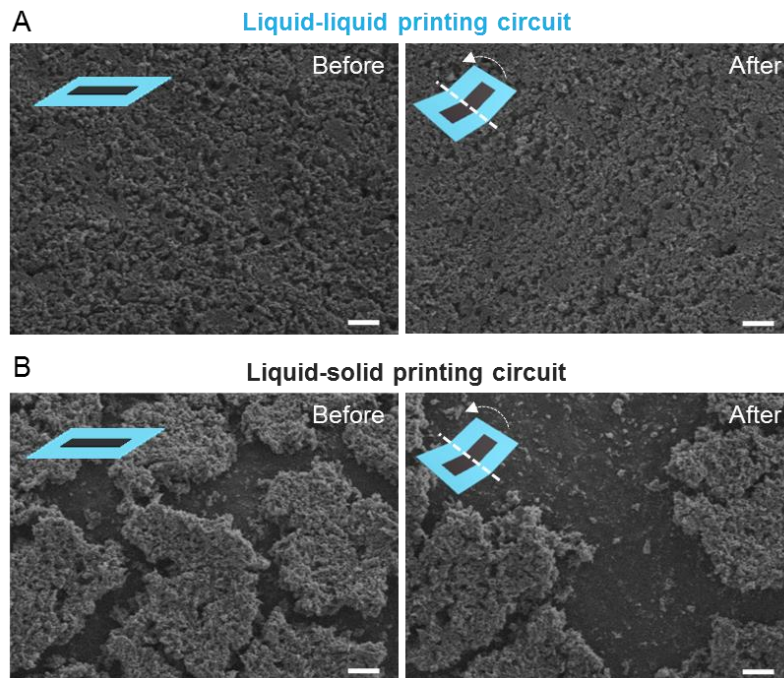


Figure S10. SEM images of liquid-liquid printing circuits (A) and liquid-solid printing circuits (B) before and after bending to 120°. Scale bar: 50 μm . Related to Figure 4.

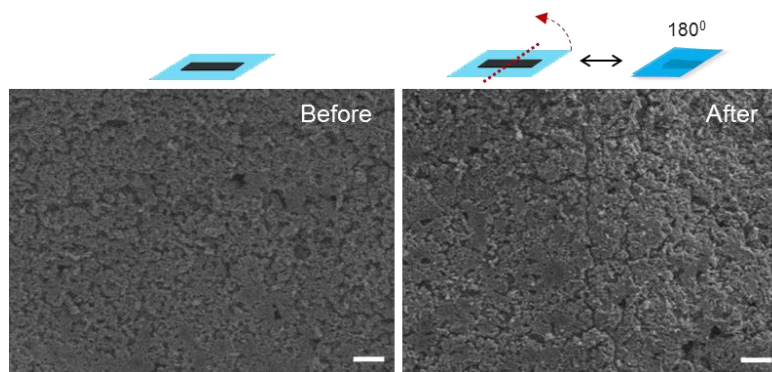


Figure S11. SEM images of liquid-liquid printing circuits before and after 1000 cycles bending to 180°. Scale bar: 50 μm . Related to Figure 4.

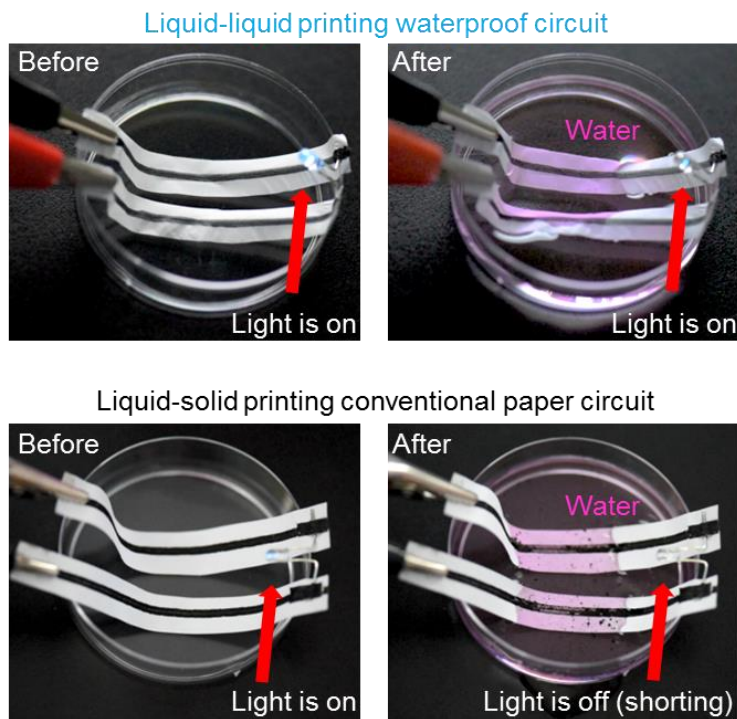


Figure S12. Waterproof of circuits based on the liquid-liquid printing technique *vs.* the conventional paper circuit. The water is the electrically conductive tap water. Comparing with the conventional paper circuit, waterproof circuit based on the liquid-liquid printing technique is much more stable. Related to Figure 4.

Table S1. Common properties of the donor liquids. Related to Figure 1.

No.	Donor liquids	Source	Density (g/mL)	Viscosity (mPa s)	CA ($^{\circ}$)	γ (mN/m)
1	Aqueous Rhodamine B	Lab-made	1.00	1.6	84.3	63.2
2	Neutral pen ink	Commercial	1.06	13.9	64.6	35.0
3	Aqueous fluorescent ink	Commercial	1.09	26.7	75.8	37.3
4	Aqueous ferrofluid	Commercial	1.39	94.1	91.2	58.3
5	Conductive donor	Lab-made	0.97	163.0	58.7	33.9

CA, contact angle. γ , surface tension, 25 $^{\circ}$ C.

Table S2. Liquid properties in Figure 2. Related to Figure 2.

Liquids	Solvents	Solutes	Density (g/mL)	Volatilization rate (mg/min)	γ (mN/m)
RB (Water)	Water	Rhodamine B	1.00	0.84	60.98
SY (Water)	Water	Sunset yellow	1.01	0.86	71.33
CM (Water)	Water	Carmine	1.01	0.77	70.41
RB (FA)	Formic acid	Rhodamine B	1.22	1.40	38.71
SY (FA)	Formic acid	Sunset yellow	1.21	0.85	38.75
RB (DMAC)	Dimethylacetamide	Rhodamine B	0.95	0.33	34.77
SY (DMAC)	Dimethylacetamide	Sunset yellow	0.95	0.26	34.34
SD (DMAC)	Dimethylacetamide	Sudan red II	0.95	0.20	34.81
SD (DMF)	Dimethylformamide	Sudan red II	0.99	0.54	36.71
RB (GLY)	Glycerin	Rhodamine B	1.27	0.00	62.31
SY (GLY)	Glycerin	Sunset yellow	1.28	0.00	63.57
SD (SO)	Shell oil	Sudan red II	0.81	0.00	28.16
PVP (FA)	Formic acid	Polyvinylpyrrolidone	1.24	1.03	38.73
PVB (Ethanol)	Ethanol	Polyvinyl butyral	0.83	1.19	22.83
PLA (DCM)	Dichloromethane	Polylactic acid	1.52	4.47	36.13
PS (THF-DMF)	Tetrahydrofuran, dimethylformamide	Polystyrene	1.03	0.25	36.26
PVDF (Acetone-DMAC)	Acetone, Dimethylacetamide	Polyvinylidene fluoride	0.92	0.21	29.22

RB: Rhodamine B; SY: sunset yellow; CM: carmine; SD: Sudan red; GLY: glycerin; SO: shell oil. DMAC: dimethylacetamide; THF: tetrahydrofuran; DMF: dimethylformamide; DCM: dichloromethane; FA: formic acid; PVDF: polyvinylidene fluoride; PS: polystyrene; PLA: polylactic acid; PVB: polyvinyl butyral; PVP: polyvinylpyrrolidone. γ , surface tension, 25 °C.

Table S3. Soluble levels of the donor solutes. Related to Figure 2.

	RB	SY	CM	SD
FA	5	5	5	5
Ethanol	5	2	2	4
DCM	5	1	1	5
THF-DMF	5	5	2	5
Acetone-DMAC	5	5	4	5

“1” denotes insoluble, “2” poor solubility, “4” unstable dissolution, and “5” dissolving completely. RB: Rhodamine B; SY: sunset yellow; CM: carmine; SD: Sudan red; FA: formic acid; DCM: dichloromethane; THF: tetrahydrofuran; DMF: dimethylformamide; DMAC: dimethylacetamide.

Table S4. The receding angle (°) of the donor liquids. Related to Figure 2.

	PVDF (Acetone-DMAC)	PS (THF-DMF)	PLA (DCM)	PVB (Ethanol)	PVP (FA)
RB (Water)	57.6	0	61.2	46.8	0
SY (Water)	48.6	0	36	37.8	0
CM (Water)	64.8	12.6	34.2	0	0
RB (FA)	32.4	0	0	0	0
SY (FA)	0	0	0	0	0
RB (DMAC)	0	0	0	0	0
SY (DMAC)	0	0	0	0	0
SD (DMAC)	0	0	0	0	0
SD (DMF)	0	0	0	0	0
RB (GLY)	0	0	97.2	0	0
SY (GLY)	0	0	55.8	0	0
SD (SO)	0	0	39.6	0	0
Water (RB)	57.6	0	61.2	46.8	0

PVDF: polyvinylidene fluoride; PS: polystyrene; PLA: polylactic acid; PVB: polyvinyl butyral; PVP: polyvinylpyrrolidone; DMAC: dimethylacetamide; THF: tetrahydrofuran; DMF: dimethylformamide; DCM: dichloromethane; FA: formic acid; RB: Rhodamine B; SY: sunset yellow; CM: carmine; SD: Sudan red; GLY: glycerin; SO: shell oil.

Table S5. Values of parameters used in the simulations in Figure 3. Related to Figure 3.

	Value	Unit	Description
c_0	0.83	Dimensionless	Mass ratio of L_{RS} to L_R in L_R flow
τ	0.00294	g/s	Mass evaporation rate of L_{RS}
k	0.001195	g/s	Mass flow rate of L_R
D_{1solv}	1×10^{-9}	m^2/s	Diffusion coefficient of the pure L_{DS} in the L_{RS}
D_{1poly}	1×10^{-12}	m^2/s	Diffusion coefficient of the pure L_{DS} in the L_{RP}
$D_0(c)$	0	m^2/s	Diffusion coefficient of ink solute in L_R
r	0.4	Dimensionless	Ratio of diffusion coefficient of ink solute and L_{DS}
Z_0	5	Dimensionless	Lower critical value in ink diffusion function
Z_1	15	Dimensionless	Upper critical value in ink diffusion function
c_{cri}	0.11	Dimensionless	Critical mass ratio of L_{RS} to L_R

L_R , the receiver liquid, was prepared by dissolving PVDF (L_{RP}) in acetone/DMAC (L_{RS}).

Table S6. Mass ratio of the receiver solvent to the overall receiver during electrospray.

Related to Figure 3.

Injection rate (mL h ⁻¹)	T (min)	Solvent (g)	Polymer (g)	<i>c</i>
3.0	6.0	0.0016	0.024	0.0625
	10.0	0.0050	0.043	0.1042
	20.0	0.0087	0.085	0.0928
	40.0	0.0234	0.183	0.1134
	50.0	0.0293	0.222	0.1166
5.1	6.0	0.0209	0.048	0.3033
	10.0	0.0497	0.078	0.3892
	20.0	0.0778	0.142	0.3540
	40.0	0.2322	0.325	0.4167
	50.0	0.1874	0.374	0.3338

c is the mass ratio of the receiver solvent (acetone/dimethylacetamide 1:1) to the overall receiver (polyvinylidene fluoride).

Transparent Methods

Materials

The materials including polyvinylidene fluoride (PVDF, M.W. 500,000, Solvay), polyvinylpyrrolidone (PVP, M.W. 130,000, Aladdin), polystyrene (PS, M.W. 100,000, Xiya), polyvinyl butyral (PVB, M.W. 9,000-120,000, Aladdin), polylactic acid (PLA, M.W. 60,000, Aldrich), polyacrylonitrile (PAN, M.W. 150,000, Sigma), graphite nanoplatelet aqueous (Aladdin), and graphene (Aladdin). N,N-Dimethylacetamide (DMAC), acetone, ethanol, tetrahydrofuran (THF), dimethylformamide (DMF), dichloromethane (DCM), and formic acid (FA) of analytical grade were obtained from Sinopharm Chemical Reagent Co., Ltd. All solutions were prepared with Milli-Q water (18.2 M Ω cm).

Donor preparation

The donor liquids include two types: one is lab-made simple, for example, an aqueous Rhodamine B (RB) donor liquid in Figure S1; the others are complex fluids, including inks in commercial pen refills (Figure S4B), lab-made composite solutions, and lab-made suspensions (Figure S9A). RB aqueous solution used in Figure S1 was prepared by dissolving RB powders in water with a final concentration of 0.1 mg mL⁻¹. For a conductive donor preparation, the graphene powders were dispersed in graphite nanoplatelet aqueous with a concentration of 10 mg mL⁻¹. The PVP was dispersed in ethanol with a concentration of 8% (wt/v). The two above mentioned solutions were mixed thoroughly under ultrasound to obtain the conductive donor (Figure S9A, Movie S2). Common properties of the donor liquids are listed in table S1.

Donor patterns preparation

The donor pattern was drawn onto the surface of a substrate by using a lettering robot

manipulator (Steamduino, China) with multiple donor liquids. A neutral pen (MG-2180, M&G Chenguang, China) was used in the experiments in Figure 3 and the black outlines of the colorful printing in Figure 4C and Figure S7B. The density and viscosity of the donor liquid are 1.06 g mL^{-1} and 13.9 mPa s at 0.1 s^{-1} shear rate, respectively (see Figure S4B). A neutral red pen (Deli 34567#, DeLi Group Co., Ltd., China) is used in Figure 1B. And the density of the ink is 1.05 g mL^{-1} . Aqueous fluorescent pens (Uni, PUS-102T, Japan) are used in Figure 4A and 4B, Figure S5, and Movie S1. Watercolor pens (ZCP24308, M&G Chenguang, China) with water-based color dyes are used for the colorful areas in Figure 4C and Figure S7B.

For the preparation of the flexible circuits, a conductive donor was contained in a syringe (2.5 mL) attached to a micro nozzle (23G). A Harvard Apparatus PHD ULTRATM Syringe Pump was used to extrude the conductive donor liquid onto the surface of an aluminum foil (surface energy 38.9 mN/m), solid PVDF (surface energy 32.6 mN/m) or A4 paper (for preparing conventional paper circuit in Figure S12) with a flow rate of $100 \text{ }\mu\text{L min}^{-1}$.

Receiver liquids preparation

PVDF (acetone-DMAC) was chosen for a typical receiver liquid, because of its high compatibility with various types of liquid donors (see Figure 2A). The PVDF (acetone-DMAC) solution (8% wt/v, density 0.89 g mL^{-1} , viscosity 194.0 mPa s at 0.1 s^{-1} shear rate, Figure S4A) was prepared by dissolving PVDF in acetone/DMAC (1:1). The fabricating process was performed with an ET-2535H electrospray machine (ET-2535H, Ucalery, China). The solution was injected through a 20G needle (injection rate $0.085 \sim 12.0 \text{ mL h}^{-1}$, applied voltage $8 \sim 13 \text{ kV}$, the distance between the tip of the needle and the

target 13 cm). PVDF solidifies during the volatilization of the receiver solvents. The whole process was conducted at 25 °C ~ 30 °C and 30% ~ 41% relative humidity for 0.1 ~ 2 h except otherwise specified. After the receiver solvent is completely volatilized, the solidification is completed. For Figure 1 B, after electro spray, both partially solidified and full solidified PVDF with transfer printed donor pattern could be easily detached from the substrate. A scanning electron microscope (SEM) image of the solid state of PVDF is shown in Figure S3D. Other receivers (Table S2) include 20% (wt/v) polystyrene with THF/DMF 1:1, 12% (wt/v) PLA with DCM, 6% (wt/v) PVB with ethanol, 10% (wt/v) PVP with FA.

In Figure 3B, we set a series of injection flow rates from 0.7 mL h⁻¹ to 12.0 mL h⁻¹ and the total injection volumes remain at 0.857 mL. Optical photos were taken to record the line width before and after the electro spray. In Figure 3C, the injection flow rate was set to 5.1 mL h⁻¹. Optical photos were taken to record the line width in real time (from 0 min to 51.5 min). For Figure S1, PVDF (acetone-DMAC) was first prepared according to the typical electro spray process described above. After the contact of RB liquid donor and the PVDF (acetone-DMAC) receiver, absorbent papers were used to absorb the excess RB liquid above. The printing process was operated in air with continuous volatilization of the receiver solvents. The PVDF was solidified along with the volatilization of the receiver solvents. The PVDF is full solidified when the solvent is completely volatilized. Then the printed materials were rinsed with DI water for three times and were dried in air.

Flexible circuits preparation

For liquid-liquid printing (LLP) circuit materials, the solutions were 8% ~ 12% (wt/v)

PVDF with the injection rate 10 mL h^{-1} for 10 ~15 min following by 3.5 mL h^{-1} for 40 min. For waterproof circuits' preparation, after the LLP circuit was peeled off from the aluminum foil, we turned them over for another electrospray process (injection rate 3.5 mL h^{-1} for 40 min). The obtained waterproof circuit (thickness $\sim 85 \text{ }\mu\text{m}$) was encapsulated between two layers of PVDF. For liquid-solid printing circuits, the conductive donor was directly written on the surface of PVDF (Movie S2).

Characterizations

The viscosity of the liquids was measured at $25 \text{ }^\circ\text{C}$ using Rheo-Microscope MCR302 (Anton Paar Co., Austria). Viscosities as well as other common properties of our donor liquids were summarized at Table S1. Liquids volatilization rate tests were measured with $\sim 10 \text{ }\mu\text{L}$ liquid vaporizing in air to demo the electrospray process, at 25°C and $38\% \pm 3\%$ relative humidity. The liquids were dropped onto aluminum foils with an area of $3 \text{ cm} \times 3 \text{ cm}$. The volatilization time was recorded until the liquids totally drying. The volatilization rate is the loss of weight of the liquids per minutes. The special affinity is denoted for the receding angle (Wang et al., 2015) divided by the solubility level of the donor solute in the receiver liquid (Table S3). For the tests of the soluble levels of the donor solutes in the receiver solvents, 2.0 mg donor solutes were added into 5.0 mL solvent following whirlpool concussion to full dissolution ($22 \text{ }^\circ\text{C}$).

The relative conductance of the printing circuits was obtained by using a source meter (2400, Keithley, USA). A voltage of 10 V was applied to the graphene line with the length of 3.5 cm and the width of 2 mm , and the current value was recorded. Fluorescent images were obtained by a TCS SP5 beam scanning confocal microscope (Leica Microsystems CMS GmbH, Germany). Zoomed-in view of the surface

morphology of the LLP and LSP circuits (Figure 4G right) was performed by a laser microscopic system (Keyence, VK-X250K). The SEM images were obtained by a field-emission scanning electron microscope Hitachi s-4800 (Hitachi, Japan). The contact angle and the receding angle measurements were performed by a contact angle measurement system OCA100 (Dataphysics, Germany) at room temperature (*i.e.*, 20 °C ~ 25 °C) with ~ 22% relative humidity (Sheng et al., 2018). During the measurements, small droplets of water (5 µL) were placed on multiple areas on the surface of the samples. Surface tension and surface energy were measured by the pendant drop method and the Owens, Wendt, Rabel and Kaelble (OWRK) method (Owens and Wendt, 1969), respectively. For the receding angle measurements (Wang et al., 2015), the receiver liquids were first placed on the aluminum foil following by contact with the donor liquids. The value of the contact angle, the receding angle and the surface tension was an average of at least three independent measurements.

Stability tests

The liquid-liquid printed materials were immersed into 1M HCl, 1M NaOH, boiling water or 95% alcohol for 10 min. The immersion time for 36.5% NaCl was two days. After the treatment, the printed materials were drawn from the solutions and rinsed with DI water for 5 min.

Theoretical modeling

We define c_0 as the mass ratio of the L_{RS} in the sprayed L_R flow. When L_R is sprayed with the mass flow rate k , the solvent (L_{RS}) in L_R partly evaporates while all polymers (L_{RP}) stay on the surface of the substrate. Here, the mass evaporation rate of L_{RS} is assumed to be a constant during the process, which is denoted as τ . The mass ratio of L_{RP}

c is different from the sprayed L_R c_0 . Here, we assume the sprayed L_R mixes uniformly with the existing solution in the substrate. From the mass conservation of L_R and L_{RS} ,

$$h(t) + kdt - \tau c(t)dt = h + dh \quad (1)$$

$$c(t)h(t) + kc_0dt - \tau c(t)dt = (c + dc)(h + dh) \quad (2)$$

where h is the mass of L_R membrane. The corresponding differential equations can be easily derived,

$$\frac{dh}{dt} = k - \tau c \quad (3)$$

$$\frac{dc}{dt} = \frac{1}{h}(kc_0 - kc - \tau c + \tau c^2) \quad (4)$$

From Fick's second law of diffusion, the governing equations for g and f are

$$\frac{\partial g}{\partial t} = \nabla(a(c)\nabla g) \quad (5)$$

$$\frac{\partial f}{\partial t} = \nabla(Z(g/f, c)\nabla f) \quad (6)$$

where g and f are the density of the donor solvent and the density of the donor ink solute, respectively, a and Z are the diffusion coefficients of donor solvent and donor ink solutes in the overall receiver. The numerical simulation is computed in COMSOL Multiphysics 5.3 with the parameters listed in Table S5 and S6. The diffusion coefficients values are the typical values of the diffusivity of the liquid in liquid and liquid in solid for the contents used in the experiments.

It needs to be mentioned that the k value in the Table S5 is proportional to the flow rate. The value of 5.1 mL h^{-1} listed in the Table S6 is used to plot Figure 3C.

Supplemental references

Owens, D.K., and Wendt, R.C. (1969). Estimation of the surface free energy of polymers. *J. Appl. Polym. Sci.* *13*, 1741-1747.

Sheng, Z., Wang, H., Tang, Y., Wang, M., Huang, L., Min, L., Meng, H., Chen, S., Jiang, L., and Hou, X. (2018). Liquid gating elastomeric porous system with dynamically controllable gas/liquid transport. *Sci. Adv.* *4*, eaao6724.

Wang, L., Li, F., Kuang, M., Gao, M., Wang, J., Huang, Y., Jiang, L., and Song, Y. (2015). Interface Manipulation for Printing Three-Dimensional Microstructures Under Magnetic Guiding. *Small* *11*, 1900-1904.